ELSEVIER

Biophysical Chemistry 101–102 (2002) 239–247

Biophysical Chemistry

www.elsevier.com/locate/bpc

Binding affinities and geometries of various metal ligands in peptide deformylase inhibitors☆

V. Madison*, J. Duca, F. Bennett, S. Bohanon, A. Cooper, M. Chu, J. Desai, V. Girijavallabhan, R. Hare, A. Hruza, S. Hendrata, Y. Huang, C. Kravec, B. Malcolm, J. McCormick, L. Miesel, L. Ramanathan, P. Reichert, A. Saksena, J. Wang, P.C. Weber, H. Zhu, T. Fischmann

Departments of Structural Chemistry, Chemical Research and Chemotherapy and Molecular Genetics, Schering Plough Research Institute, 2015 Galloping Hill Road, Kenilworth, NJ 07033, USA

Abstract

Removal of the N-terminal formyl group from newly synthesized proteins by the enzyme peptide deformylase (PDF) is essential for normal growth of bacteria but not higher organisms. Recently, PDF has been explored as a target for novel antibiotics. Screening a collection of natural products for antimicrobial activity identified actinonin and two matlystatin analogs as potent PDF inhibitors. A number of synthetic analogs of these natural products were prepared and their inhibitory potency determined. Previous work has shown that PDF is an iron metalloproteinase also containing a catalytic glutamic acid residue. Ligation of the ferrous cation is an essential feature of potent inhibitors. The structures of actinonin, a matlystatin analog and a synthetic inhibitor complexed with PDF were determined by crystallography. A quantum mechanics/molecular mechanics (QM/MM) method was used to reproduce the geometry of known complexes, to predict the protonation state in the active site and to predict the geometry of additional complexes. The requirement for protonation of the active site glutamate anion is an important factor in understanding the potency of inhibitors with acidic iron-ligating groups such as hydroxamate and carboxylate. Even though potent inhibitors of PDF have been discovered, their bacteriostatic mechanism of action and the rapid development of resistance in vitro may limit their potential as antibacterial drugs.

Keywords: Actinonin; Antibiotics; Crystallographic structures; Matlystatin

☆ I dedicate this paper to Professor John Schellman for his seminal role in my scientific development, his continued support and friendship. The biophysical philosophy that John taught and exemplified at the University of Oregon has been a cornerstone of my career. I am grateful for his guidance that catalyzed my transition from novice student to research scientist (from Vincent Madison).

*Corresponding author.

E-mail address: vincent.madison@spcorp.com (V. Madison).

0301-4622/02/$ - see front matter
PII: S0301-4622(02)00179-5

1. Introduction

Effective antibiotic therapy with minimal toxicity can be best achieved by selecting targets that are essential to the pathogen, but absent in the host organism. In bacteria, initiation of protein synthesis requires transfer of a formyl group from N^{10}-formyltetrahydrofolate to methionine bound to transfer-RNA_f^{Met} by the enzyme transformylase (Fmt). Subsequent deformylation of proteins catalyzed by peptide deformylase (PDF) is essential for bacterial growth. The formylation/deformylation pathway is not a general feature of protein synthesis in higher organisms, but deformylase genes have been identified in cells of higher plants and humans [1]. Nevertheless, PDF has many properties that make it an attractive target for antimicrobial agents [2].

PDF is a metalloprotease containing a ferrous cation chelated by two imidazoles and a thiol. The two imidazoles and a catalytic acid residue occur in a α-helical HEXXH motif [3,4] in common with the zinc metalloprotease superfamily (metzincins). There are both similarities and differences in substrate recognition between PDF and metzincins [5]. The binding modes of a formyl-peptide hydrolysis product and two inhibitors have been revealed in crystal structures [3,6].

It has been shown that actinonin, a naturally occurring antibacterial agent, is a potent PDF inhibitor and that this inhibition is the mechanism of its bacteriostatic activity [7]. Several groups have discovered PDF inhibitors from screening compound collections and have prepared analogs. The most potent inhibitors contained a hydroxamate group as the iron ligand [8,9]. Other inhibitory ligands included tetrazoles [10], *N*-hydroxyureas, hydrazides [8] and hydroxyformamides [6].

Our screening of natural products for PDF inhibitors, identified actinonin and two matlystatin analogs containing carboxylate and hydroxamate ligands, respectively. Additional synthetic analogs containing hydroxamate, carboxylate, hydroxyformamide and amide ligands were prepared and assayed. Crystal structures were determined for Fe^{2+}-PDF complexed with hydroxamate and carboxylate ligands. Quantum mechanics/molecular mechanics (QM/MM) methods were calibrated versus known structures, then geometries of novel complexes and protonation states in the active site were predicted.

2. Experimental

The purification of *E. coli* Fe^{2+}-PDF followed the procedure of Rajagopalan et al. [11] except that oxyrase and catalase were added to all buffers to prevent enzyme oxidation [12]. Inhibition constants were determined using the continuous assay of Wei and Pei [13] at pH 7.2 with minor adaptations including the addition of oxyrase and catalase [12]. Steady state reaction velocities were used to calculate inhibition constants (K_i^*) of reversible slow-binding inhibitors as described by Morrison and Walsh [14]. Prior to crystallization, the oxyrase and catalase concentrations were reduced 10-fold by ultracentrifugation to prevent precipitation of these enzymes. Using conditions that have been described, crystals were obtained with the reported space group [15], but with significantly higher resolution, up to 1.25 Å. The structure was solved by molecular replacement from pdb entry 1DFF using the program AMORE (CCP4) [16], and refined using the program BUSTER [17]. Data collection and refinement statistics are given in Table 1.

For computations of optimum geometry and protonation states in the PDF active site, the frozen orbital-based QM/MM method developed by Schrödinger, Inc. [18,19] was used. The QM region included the metal ion (Fe^{2+}), the complete His^{132} and Glu^{133} residues, and the sidechains of His^{136} and Cys^{90}. Each inhibitor was also part of the QM region. The QM method used was B3-LYP DFT using 6-31G* basis sets for all atoms except that LACVP* effective core potentials were used for iron [20]. All coordinates in the QM region were free to adjust during the optimization. The remaining residues in a 10 Å sphere around the binding site comprised the MM region. All coordinates were frozen at their experimental values in the MM region except those of Met^{134}.

3. Results

To identify inhibitors, the naturally occurring ferrous form of PDF was screened against our

novel collection of natural products. Two new matlystatin analogs (**4A**, **4C**) were discovered in addition to actinonin (**1A**) that had been described previously (Fig. 1). Numerous synthetic analogs were prepared based on the structures of these natural products and of PDF/inhibitor complexes. This report focuses on inhibitors that permit direct comparisons of potency among various iron-ligating groups as well as comparisons of crystallographic and computed structures. The hydroxamates (**1A**–**5A**) were potent inhibitors with K_i^* values ranging from 0.1 to 3.0 nM (Table 2). The hydroxyformamides (**3B**, **5B**) were approximately 4-fold less potent. Compared to the parent hydroxamates, the carboxylates (**1C**, **2C**, **5C**, **6C**) were ~2000-fold less potent while **3C** and **4C** were only 200-fold less potent. The carboxamide **2D** was 15 000-fold less potent than its parent.

The inhibitor positions are well defined in crystal structures of PDF/inhibitor complexes. The electron density for the matlystatin analog **4C** is clearly defined, but has a small break near the isopropyl sidechain of the terminal ethylketo-valine residue (Fig. 2). The ligation and hydrogen bond geometries are reported for three inhibitors and compared to those in two published structures. The Fe^{2+}-PDF/actinonin (**1A**) complex has bidentate chelation of iron by the hydroxamate group with both Fe–O distances 2.1 Å. Short distances indicate strong Hbonds between $Glu^{133}O^{\varepsilon 1}$ and the hydroxamate NH and between $Glu^{133}O^{\varepsilon 2}$ and the hydroxamate O(H). The hydroxamate CO makes weaker Hbonds to the backbone NH of Leu^{91} and the sidechain NH_2 of Gln^{50} (Fig. 3a). The published Ni^{2+}–PDF/actinonin complex is virtually identical to the Fe^{2+}-PDF/actinonin complex, but a few distances change by 0.1–0.2 Å (Fig. 3b). Reversing the positions of the carbonyl and hydroxylamine groups (Fig. 3c) causes a shift of Glu^{133} to increase the CH–$O^{\varepsilon 1}$ distance to 3.1 Å compared to 2.6 Å for the NH–O distance (Fig. 3b) [6]. There is a strong $Glu^{133}O^{\varepsilon 2}$–OC Hbond and weak NO–$Leu^{91}$NH and $Gln^{50}NH_2$ Hbonds. The carboxylic acid (Fig. 3d) forms a

Table 2
Inhibition of *E. coli* PDF

Cpd/R[a]	**A**		**B**		**C**		**D**	
	Ki*[b]	Rel[c]	Ki*	Rel	Ki	Rel	Ki	Rel
1	0.3	1	–	–	1200	4000	–	–
2	0.1	1	–	–	180	1800	1500	15 000
3	0.3	1	2.0	7	60	200	–	–
4	0.3	1	–	–	60	200	–	–
5	3.0	1	4.0	1	4000	1300	–	–
6	0.2	1	–	–	250	1200	–	–

[a] Structures are given in Fig. 1.
[b] Inhibition constant in nM units.
[c] Ki relative to parent hydroxamate (**A**).

Table 1
Data collection and refinement statistics

	PDF-Cpd **1A**	PDF-Cpd **4C**	PDF-Cpd **6C**
Resolution (Å)[a]	1.5 (1.51–1.50)	1.9 (1.92–1.90)	1.8 (1.82–1.80)
Measured reflections	1 167 060	747 519	645 157
Unique reflections	91 008	48 541	56 866
Completeness (%)	91.5 (80.3)	87.0 (40.4)	98.1 (98.3)
R_{sym}(%)[b]	4.0 (14.3)	5.8 (20.6)	6.2 (32.5)
$\langle I \rangle / \sigma_I$	23.9 (5.7)	19.5 (4.5)	18.5 (3.7)
R_{work}[c]	18.6	19.5	20.3
R_{free}(%)[d]	20.2	23.6	23.5
Alternate locations	77	12	46
Nb of atoms	4528	4689	4505

[a] Number between parentheses are for the outer resolution shell.
[b] $R_{sym} = \sum_h \sum_i |I_{hi} - I_h| / \sum_{hi} I_{hi}$ where h are unique reflection indices and I_{hi} are the intensities of symmetry equivalent reflections giving a weighted mean of I_h.
[c] $R = \sum |F_{obs} - F_{calc}| / S\, F_{obs}$ where F_{obs} and F_{calc} are observed and atomic model structure factor amplitude, respectively.
[d] R_{free} calculate for 5% of randomly chosen reflections that were excluded from gradient estimates in refinement calculations.

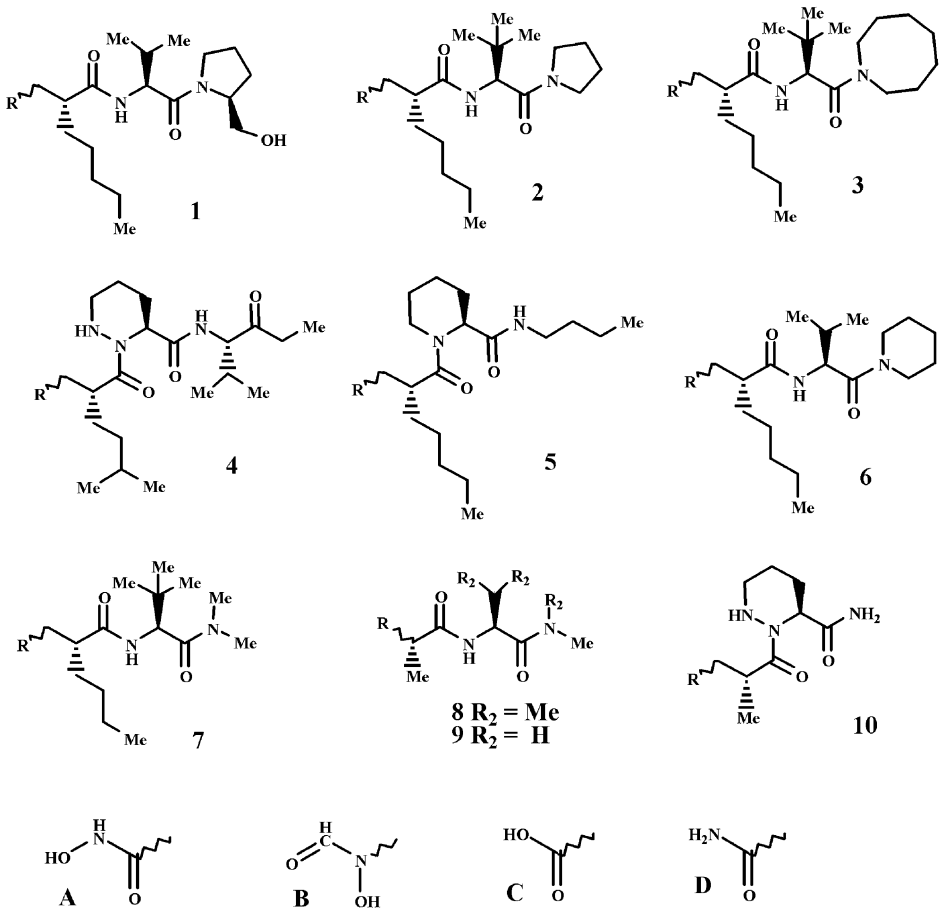

Fig. 1. Chemical structures of compounds divided into common scaffolds (**1**–**10**) and metal binding head groups (**A**–**D**). Inhibition data are reported for scaffolds (**1**–**6**), scaffold (**7**) is in a crystal structure [6], and scaffolds (**8**–**10**) were used for QM calculations as simplifications of actual compounds.

monodentate complex with a Fe–O^1 distance of 2.0 Å. There is a strong $Glu^{133}O^{\varepsilon 1}$–$O^2$ Hbond and weak NH Hbonds to O^1. In the complex of PDF with another inhibitor with a carboxylic acid ligand (Fig. 3E), the carboxylate is shifted so that O^2 now ligates iron with a Fe–O^2 distance of 2.0 Å. The $Glu^{133}O^{\varepsilon 1}$–$O^2$ distance increases to 2.8 Å in this complex, still indicative of a strong Hbond. There are weaker Hbonds from protein NH groups to O^1.

QM/MM density functional methods have provided useful insights on structures, reactivities and reaction mechanisms in metalloenzymes [21] and on the influence of the protein environment on bonding to iron in myoglobin [22]. Comparing the computed optimized geometry with that observed crystallographically for four of the inhibitors will test the validity of the methods for PDF. QM/MM calculations were performed using the simplified scaffold **8** with all four metal-ligating head groups **A**–**D**, using compound **10C** and a transition state model based on scaffold **9**. The calculations reproduced the experimental geometry well for the PDF/inhibitor complexes. The RMSDs for the heavy atoms of the head groups (as defined in Fig. 1 plus the C^{α}) vary from 0.4 to 0.8 Å (Table 3). The calculated Hbond distances are approximately 0.4 Å longer than those observed. The

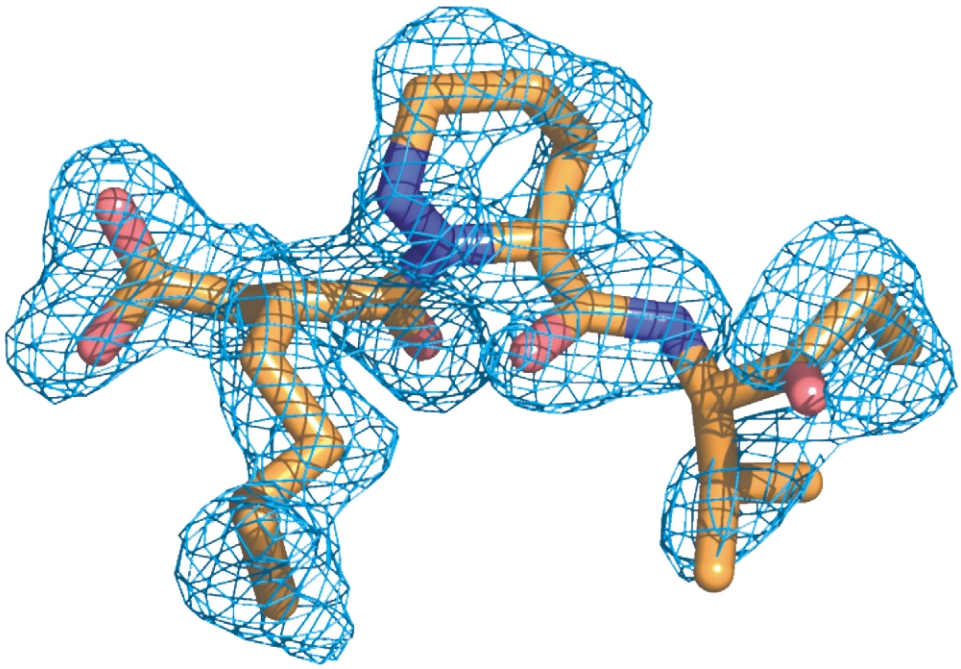

Fig. 2. Electron density around matlystatin analog **4C** from maximum entropy omit map contoured at 2.5σ. In the stick representation, oxygens are red, nitrogens blue and carbons orange.

calculated Fe–O ligand distances are approximately 0.2 Å shorter than observed except that bidentate ligation with equal Fe–O distances is predicted for carboxylate while monodentate ligation is observed with the second Fe–O distance 0.7 Å longer. This good agreement of the structures lends credence to the QM/MM predictions of protonation states in the active site and of geometries for novel ligands. The computations predict transfer of the acidic OH protons of hydroxamic acids and hydroxyformamides to $Glu^{133}O^{\varepsilon 2}$ (Fig. 4a and c). For carboxylate ligands, a proton is predicted on $Glu^{133}O^{\varepsilon 1}$ consistent with the observed glutamate–carboxylate Hbond (Fig. 4d and e). For the carboxamide head group, a short Fe–O distance is predicted. However, the Hbond angles between the NH_2 group and Glu^{133} are non-ideal. There is also an unfavorable short NH–Fe distance consistent with the low potency of inhibitor **2D** (Fig. 4f). For comparison to the inhibitors, the tetrahedral intermediate formed by the addition of a water molecule to a peptide formamide was also modeled. The two water protons are transferred to $Glu^{133}O^{\varepsilon 2}$ and the formamide NH, respectively. The double oxyanion is stabilized by bidentate ligation to Fe^{2+} and by Hbonds to $Leu^{91}NH$, $Gln^{50}NH_2$ and $Glu^{133}O^{\varepsilon 2}H$. The ammonium cation Hbonds to $Glu^{133}O^{\varepsilon 1}$ and $Gly^{45}CO$ (Fig. 4g).

4. Discussion

The hydroxamate ligand fits well the geometric and chemical requirements of the PDF active site with bidentate iron ligation, two Hbonds to Glu^{133} and two CO–NH Hbonds. This complex closely mimics several features of the tetrahedral intermediate formed when an activated water molecule attacks the N-terminal formamide group during the enzymatic reaction. Both complexes have bidentate iron ligation, two Hbonds to Glu^{133} and two more Hbonds to $Leu^{91}NH$ and $Gln^{50}NH_2$. In the tetrahedral intermediate, the ammonium group makes an additional Hbond to $Gly^{45}CO$. The hydroxyformamide ligand is very

similar to hydroxamates except that the strong NH–$O^{\varepsilon 1}$ Hbond is replaced by a weak CH–$O^{\varepsilon 1}$ interaction. This difference is primarily responsible for the ~4-fold weaker binding of the hydroxyformamide inhibitors reported here. A review of MMPs reports a generic reduction of ~10-fold [23]. Both ligands would retain their weakly acidic proton at neutral pH and transfer it from their hydroxylamine groups to the Glu^{133} carboxylate upon binding. This proton transfer predicted by the QM/MM calculations is consistent with lowering the pK_a of the bound ligand and the raised pK_a of the active site glutamic acid in metalloproteinases (J.B. Cross, J.S. Duca, J.J. Kaminski and V.S. Madison, The active site of a zinc-dependent metalloproteinase influences the computed pK_a of ligands coordinated to the catalytic zinc ion, to be published).

The carboxylic acid inhibitors make fewer interactions with PDF. They have monodentate iron ligation and a single Hbond to Glu^{133}. The bidentate ligation predicted by the QM/MM calculations is the major discrepancy with experimental structures. Both the inhibitor and Glu^{133} carboxylates would be predominately ionized at neutral pH; one would need to be protonated in order to form the strong Hbond observed crystallographically. For Co^{2+}-PDF, Rajagopalan et al. have reported a pH activity profile that shows titration of a single active site group with a pK_a of ~5.2 which is assigned to Glu^{133}. The metal bound water molecule is not ionized; absorption spectra of wildtype Co^{2+}-PDF have shown only water (not hydroxide)

Table 3
RMSD (Å) of crystallographic inhibitor structures and QM/MM optimized geometries for model compounds

Inhibitor	Model	RMSD
1A	**8A**	0.6
7B	**8B**	0.4
4C	**10C**	0.5
6C	**8C**	0.8

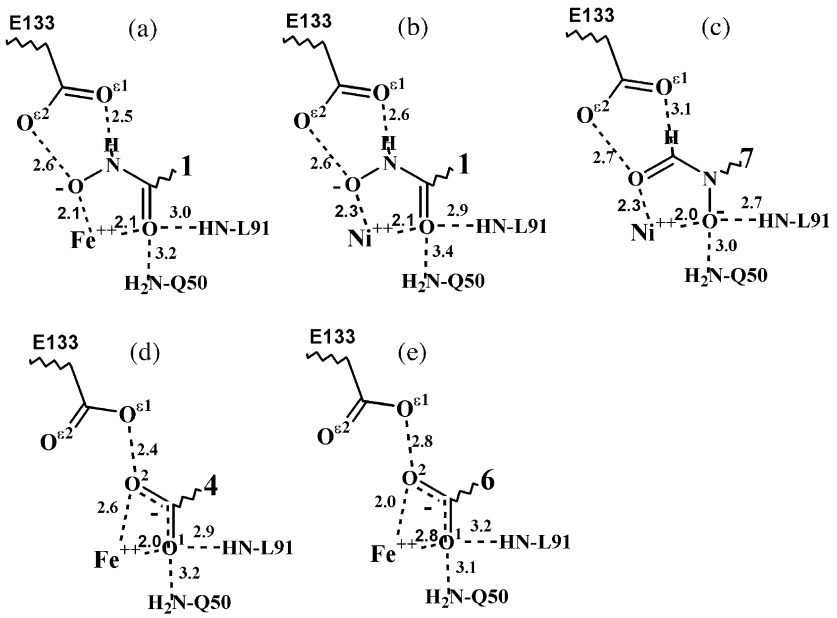

Fig. 3. Metal ligation and hydrogen bonding of various head groups in the PDF active site from X-ray crystallography. Interatomic distances for heavy atoms are given in Å. The values for **A**–**C** are averages for the three molecules in the asymmetric unit. Structures **B** and **C** are from Ref. [6]. QM calculations indicate that E133 is protonated while the metal ligands are anions. Compounds are defined in Fig. 1: (a) Compound **1A**; (b) Compound **1A**; (c) Compound **7B**; (d) Compound **4C**; and (e) Compound **6C**.

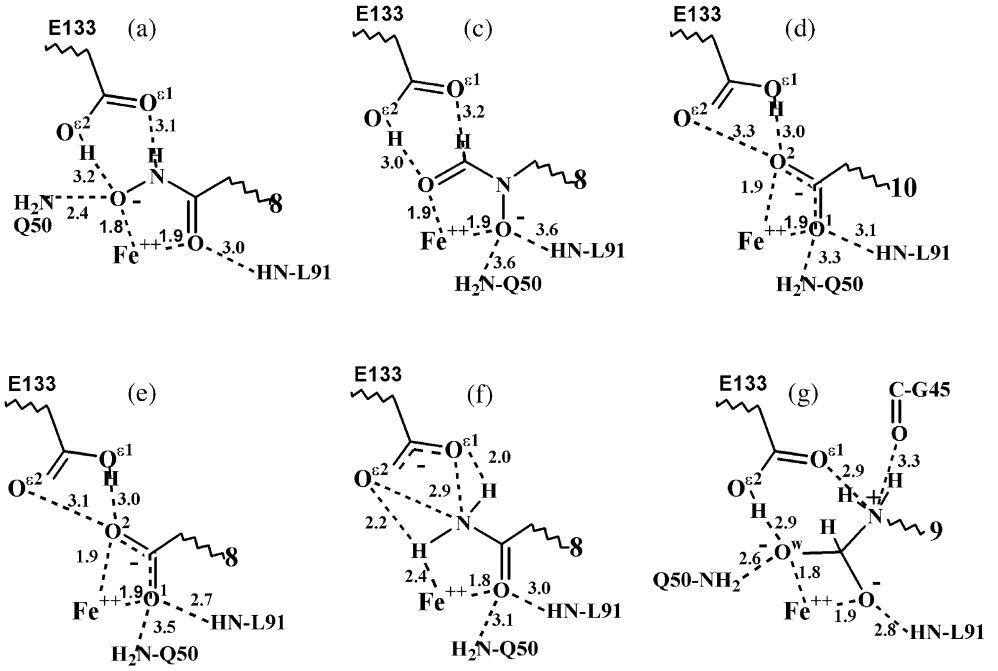

Fig. 4. Geometry of various head groups in the PDF active site in the optimized geometry from QM/MM calculations. **A**, **C**, **D** and **E** represent model compounds corresponding to experimental structures in Fig. 3 **A**, **C**, **D** and **E**. Interatomic distances (Å) are between heavy atoms to facilitate comparison to Fig. 3, except for F which includes distances to the protons of the carboxamide. Simplified scaffolds **8**, **9** and **10** were used. Models and inhibitors are defined in Fig. 1: (a) model **8A**, hydroxamate inhibitor **1A**; (c) model **8B**, hydroxyformamide inhibitor **B**; (d) model **10C**, carboxylate inhibitor **4C**; (e) model **8C**, carboxylate inhibitor **6C**; (f) model **8D**, carboxamide inhibitor **2D**; (g) model **9** plus head group given here to form a reactive tetrahedral intermediate (no real compound for comparison).

as a metal ligand [24]. Glu^{133} would be only 1% protonated at the pH of 7.2 utilized for measurement of the inhibition constants reported herein. The carboxylate inhibitors (**1C**, **2C**, **5C**) were ~2000-fold less potent than their parent hydroxamates. This difference can be partitioned into a 100-fold decrease due to the 1% population of PDF Glu^{133}COOH and a 10-fold decrease due to the preferential binding of hydroxamate versus carboxylate for many inhibitor scaffolds. The latter preference was eliminated in the carboxylate inhibitors **3C** and **4C** which are only ~200-fold less potent than the hydroxamates. Perhaps the increased relative potency of **4C** compared to **6C** arises from the shift in binding mode of the carboxylate (Fig. 3d and e). From a study of the pH dependence of MMP3 catalysis and inhibition, Johnson et al. [25] deduce that a carboxylate inhibitor binds to the protonated form of the active site Glu^{202} whose pK_a is 5.6. In MMPs, carboxylate inhibitors at neutral pH are also generally ~1000-fold less potent than hydroxamates [23]. For MMPs and PDF the lower potency of carboxylate inhibitors can be assigned to the requirement for protonation of the catalytic glutamic acid residue and to differences in preferred ligating geometry.

Potent inhibitors of PDF were discovered in this study and in several others. However, the antibacterial potential of these agents is limited by two factors. First, the inhibitors are bacteriostatic rather than bacteriocidal [7,20]. Second, bacterial populations contain resistance mutants at a frequency of approximately 10^{-7}. In *E. coli* [26] and *S. aureus* [27] resistance is due to mutations in the

transformylase gene so that protein synthesis is initiated without formylation of Met-$tRNA_f^{Met}$. These mutants are less fit than wildtype and show slower growth. In *S. pneumoniae*, there is a mutation in the *def* gene for PDF that directly confers resistance to inhibition [28].

References

[1] C. Giglione, A. Serero, M. Pierre, B. Boisson, T. Meinnel, Identification of eukaryotic peptide deformylases reveals universality of N-terminal protein processing mechanisms, EMBO J. 19 (2000) 5916–5929.

[2] Z. Yuan, J. Trias, R.J. White, Deformylase as a novel antibacterial target, Drug Discovery Today 6 (2001) 954–961.

[3] M.K. Chan, W. Gong, P.T.R. Rajagopalan, B. Hao, C.M. Tsai, D. Pei, Crystal structure of *Escherichia coli* peptide deformylase, Biochemistry 36 (1997) 13904–13909.

[4] A. Becker, I. Schlichting, W. Kabsch, D. Groche, S. Schultz, A.F.V. Wagner, Iron center, substrate recognition and mechanism of peptide deformylase, Nature Struct. Biol. 5 (1998) 1053–1058.

[5] S. Ragusa, P. Mouchet, C. Lazennec, V. Dive, T. Meinnel, Substrate recognition and selectivity of peptide deformylase. Similarities and differences with metzincins and thermolysin, J. Mol. Biol. 289 (1999) 1445–1457.

[6] J.M. Clements, R.P. Beckett, A. Brown, et al., Antibiotic activity and characterization of BB-3497, a novel peptide deformylase inhibitor, Antimicrob. Agents Chemother. 45 (2001) 563–570.

[7] D.Z. Chen, D.V. Patel, C.J. Hackbarth, et al., Actinonin, a naturally occurring antibacterial agent, is a potent deformylase inhibitor, Biochemistry 39 (2000) 1256–1262.

[8] A. Thorarensen, M.R. Douglas, D.C. Rohrer, et al., Identification of novel potent hydroxamic acid inhibitors of peptidyl deformylase and the importance of the hydroxamic acid functionality on inhibition, Bioorg. Med. Chem. Lett. 11 (2001) 1355–1358.

[9] C. Apfel, D.W. Banner, D. Bur, et al., 2-(2-Oxo-1,4-dihydro-2H-quinazolin-3-yl)- and 2-(2,2-dioxo-1,4-dihydro-2H-2λ^6-benzo[1,2,6]thiadiazin-3-yl)-*N*-hydroxyacetamides as potent and selective peptide deformylase inhibitors, J. Med. Chem. 44 (2001) 1847–1852.

[10] B.G. Green, J.H. Toney, J.W. Kozarich, S.K. Grant, Inhibition of bacterial peptide deformylase by biaryl acid analogs, Arch. Biochem. Biophys. 375 (2000) 355–358.

[11] P.T.R. Rajagopalan, A. Datta, D. Pei, Purification, characterization, and inhibition of peptide deformylase from *Escherichia coli*, Biochemistry 36 (1997) 13910–13918.

[12] S. Bohanon, A. Hruza, L. Ramanathan et al., Peptide deformylase of *Staphylococcus aureus*: kinetic and structural comparison to the *E. coli* enzyme, The 14th Protein Society Symposium, San Diego, CA, August 5–9, 2000.

[13] Y. Wei, D. Pei, Continuous spectrophotometric assay of peptide deformylase, Anal. Biochem. 250 (1997) 29–34.

[14] J.F. Morrison, C.T. Walsh, The behavior and significance of slow-binding enzyme inhibitors, Adv. Enzymol. Relat. Areas Mol. Biol. 61 (1988) 201–301.

[15] A. Becker, I. Schlichting, W. Kabsch, S. Schultz, A.F.V. Wagner, Structure of peptide deformylase and identification of the substrate binding site, J. Biol. Chem. 273 (1998) 11413–11416.

[16] J. Navaza, AMoRe: an automatic package for molecular replacement, Acta Cryst. A50 (1994) 157–163.

[17] G. Bricogne, The Bayesian statistical viewpoint on structure determination: basic concepts and examples, Meth. Enzymol. 276A (1997) 361–423.

[18] R.B. Murphy, D.M. Philipp, R.A. Friesner, A mixed quantum mechanics/molecular mechanics (QM/MM) method for large-scale modeling of chemistry in protein environments, J. Comp. Chem. 21 (2000) 1442–1457.

[19] R.B. Murphy, D.M. Philipp, R.A. Friesner, Frozen orbital QM/MM methods for density functional theory, Chem. Phys. Lett. 321 (2000) 113–120.

[20] P.J. Hay, W.R. Wadt, Ab initio effective core potentials for molecular orbital calculations. Potentials for K to Au including the outermost core orbitals, J. Chem. Phys. 82 (1985) 299–310.

[21] C. Rovira, B. Schulze, M. Eichinger, J.D. Evanseck, M. Parrinello, Influence of the Heme pocket conformation on the structure and vibrations of the Fe–CO Bond in myoglobin: a QM/MM density functional study, Biophys. J. 81 (2001) 435–445.

[22] K. Morokuma, D.G. Musaev, T. Vreven, H. Basch, M. Torrent, D.V. Khoroshun, Model studies of the structures, reactivities, and reaction mechanisms of metalloenzymes, IBM J. Res. Dev. 45 (2001).

[23] R.E. Babine, S.L. Bender, Molecular recognition of protein–ligand complexes: applications to drug design, Chem. Rev. 97 (1997) 1359–1472.

[24] P.T.R. Rajagopalan, S. Grimme, D. Pei, Characterization of cobalt(II)-substituted peptide deformylase: function of the metal ion and the catalytic residue Glu-133, Biochemistry 39 (2000) 779–790.

[25] L.L. Johnson, A.G. Pavlovsky, A.R. Johnson, et al., A rationalization of the acidic pH dependence for stromelysin-1 (matrix metalloproteinase-3) catalysis and inhibition, J. Biol. Chem. 275 (2000) 11026–11033.

[26] C.M. Apfel, H. Locher, S. Evers, et al., Peptide deformylase as an antibacterial drug target: target validation and resistance development, Antimicrob. Agents Chemother. 45 (2001) 1058–1064.

[27] P.S. Margolis, C.J. Hackbarth, D.C. Young, et al., Peptide deformylase in *Staphylococcus aureus*: resistance to inhibition is mediated by mutations in the formyltransferase gene, Antimicrob. Agents Chemother. 44 (2000) 1825–1831.

[28] P. Margolis, C. Hackbarth, S. Lopez, et al., Resistance of *Streptococcus pneumoniae* to deformylase inhibitors is due to mutations in *def*B, Antimicrob. Agents Chemother. 45 (2001) 2432–2435.